Chapter 3
Introduction to Depletion Interaction and Colloidal Phase Behaviour

Remco Tuinier

Abstract Efforts to explain physical properties of colloidal suspensions in terms of the forces that act between the colloidal particles go back to the beginning of the 20th century. In the second half of the last century theoretical progress clarified that the stability of colloidal particles is also affected by non-adsorbing polymers in solution, as first explained by Asakura and Oosawa in Japan using the excluded and free volume concepts. Here an introduction to the depletion interaction and resulting phase behaviour in colloidal suspensions is provided. The theory for the phase behaviour of colloidal dispersions is developed here starting from the Van der Waals theory for the as-liquid phase transition. Subsequently, the hard sphere fluid-solid phase transition is explained. Next, an attractive Yukawa hard-core model is used to outline the effects of varying the range of attraction on the phase behaviour of a colloidal suspension of attractive particles. Finally, the phase states that can be found in a colloidal hard sphere dispersion plus depletants are explained.

3.1 Introduction and Some History

3.1.1 The First Theory on Depletion Interaction

In the early 1950s the legendary Oosawa [1], at that time a young Associate Professor at Nagoya University in Japan, organized a winter symposium in Nagoya and invited a multidisciplinary group of Japanese scholars, mainly active in

R. Tuinier (✉)
Laboratory of Physical Chemistry, Department of Chemical Engineering and Chemistry and Institute for Complex Molecular Systems, Eindhoven University of Technology, 513, 5600 MB Eindhoven, The Netherlands
e-mail: r.tuinier@tue.nl

R. Tuinier
Van 't Hoff Laboratory for Physical and Colloid Chemistry, Department of Chemistry, Debye Institute, Utrecht University, Utrecht, The Netherlands

P.R. Lang and Y. Liu (eds.), *Soft Matter at Aqueous Interfaces*,
Lecture Notes in Physics 917, DOI 10.1007/978-3-319-24502-7_3

biology. Oosawa has a statistical mechanics background and he asked the group to present work on phenomena in biological systems where statistical physics could be helpful to understand certain mechanisms. During the meeting the 'aggregation' of particles under the influence of macromolecules was a re-occuring theme. It was observed in suspensions of red blood cells, bacterial cells, soil powder and gum latex particles. This inspired Oosawa to start work with Sho Asakura, then a graduate student, on the influence of polymers on the interaction between particles.

In 1953 P.J. Flory was invited by professor Yukawa to Tokyo and met Oosawa. Oosawa invited Flory to come to Nagoya University [1]. During Flory's visit Asakura and Oosawa explained their theoretical results on two particles immersed in a solution containing nonadsorbing polymer chains, showing the chains impose an *attractive* interaction between the particles. The very positive response of Flory, at that time Associate Editor of *J. Chem. Phys.* resulted in submission of this work, leading to the seminal paper in which Asakura and Oosawa [2] presented a statistical mechanical derivation of the interaction between two plates immersed in a solution of ideal nonadsorbing polymers. The theory of Asakura and Oosawa [2] is the first theoretical prediction of a depletion force. It will be explained in more detail later on. They showed that adding nonadsorbing polymer chains induce an effective attraction between particles with a hard core interaction. The attraction originates from repulsive interactions only, so it is a purely entropic effect.

This led to the discovery of the seminal Asakura-Oosawa depletion potential first published in their 1954 paper [2]. The term 'depletion' was probably introduced by Napper [3]. Oosawa indicated that the derivations and calculations were performed within a few weeks [4] and wished to note that he actually does not like the word 'depletion'.

3.1.2 Origin of the Depletion Force

The origin of the depletion effect is now first explained by regarding colloidal hard spheres in a solution of nonadsorbing polymer. The fact that polymers do not adsorb results in an effective depletion layer near the surface of the colloidal particles due to a loss of configurational entropy of a polymer chain in that region. In Fig. 3.1 a few colloidal spheres are depicted in a polymer solution. The depletion layers are indicated by the (dashed) circles around the spheres. When the depletion layers overlap the volume available for the polymer chains increases. Hence states in which the colloidal spheres are close together are more favourable. Therefore the polymers indirectly induce an effective attraction force between the spheres even though the direct colloid-colloid and colloid-polymer interactions are repulsive [5]. Vrij called this 'attraction through repulsion'.

At least in the limit of low depletant concentrations the attraction equals minus the product of the osmotic pressure and the overlap volume, indicated by the hatched region between the close spheres in Fig. 3.1. The picture sketched above became first clear in the 1950s through the work of Asakura and Oosawa [2, 6].

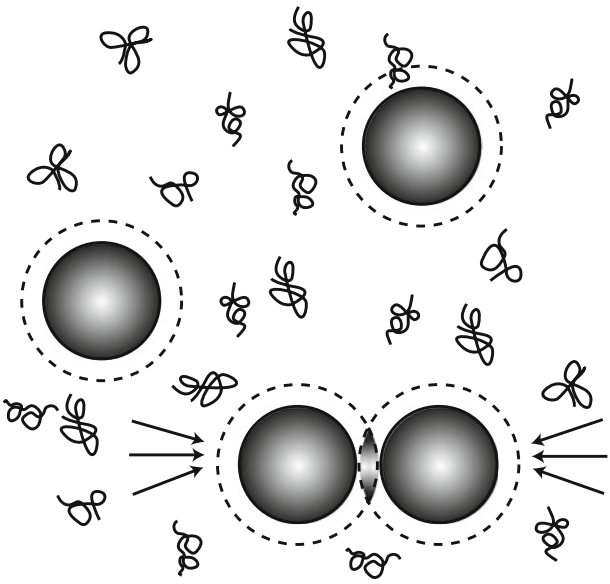

Fig. 3.1 Schematic picture of a few colloidal spheres in a polymer solution with nonadsorbing polymers. The depletion layers are indicated by the *short dashes*. When there is no overlap of depletion layers (*upper two spheres*) the osmotic pressure acting upon the spheres due to the polymers is isotropic. For overlapping depletion layers (*lower two spheres*) the osmotic pressure on the spheres is unbalanced; the excess pressure is indicated by the *arrows*

It was hardly noticed in the literature at first, seemed forgotten, but started to gain attention when Vincent et al. [7] and Vrij [5] started systematic experimental and theoretical work on colloid-polymer mixtures.

Below the standard expression used for the depletion interaction [2, 5, 6] is given. Consider two colloidal spheres each with volume $v_c = 4\pi R^3/3$ and diameter $2R$, surrounded by a depletion layer with thickness δ. In that case the depletion potential can be calculated from the product of $\Pi = n_b k_B T$, the (ideal) osmotic pressure of depletants with bulk number density n_b, times $V_{\rm ov}$, the overlap volume of the depletion layers. Hence the Asakura-Oosawa-Vrij (AOV) depletion potential equals:

$$W(h) = \begin{cases} \infty & h<0 \\ -\Pi\ V_{\rm ov}(h) & 0 \le h \le 2\delta \\ 0 & h \ge 2\delta \end{cases} \tag{3.1}$$

with overlap volume $V_{\rm ov}(h)$,

$$V_{\rm ov}(h) = \frac{\pi}{6}(2\delta - h)^2(3R + 2\delta + h/2). \tag{3.2}$$

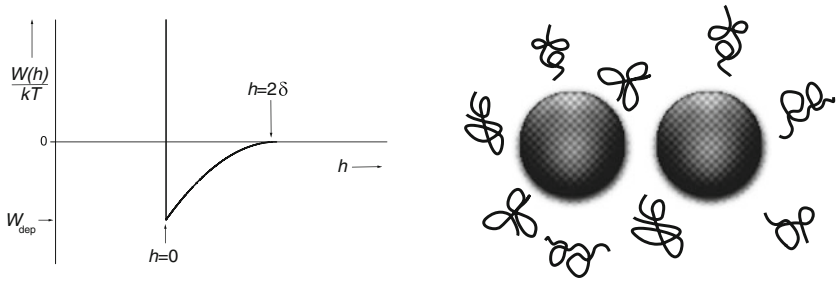

Fig. 3.2 Sketch of the depletion interaction between two hard spheres

In Fig. 3.2 the AOV interaction potential $W(h)$ is plotted. The minimum value of the potential W_{dep} is achieved when the particles touch ($h = 0$). Inspection of Eqs. (3.1) and (3.2) reveals that the *range* of the depletion attraction is determined by the size 2δ of the depletant, whereas the *strength* of the attraction increases with the osmotic pressure of the depletants, hence with the depletant concentration. Depletion effects offer the possibility to independently modify the range and the strength of attraction between colloidal particles. In dilute polymer solutions, the depletion thickness $\delta \approx 1.1R_g$ [8–10], so δ is close to the polymer's radius of gyration R_g.

It is noted that in the original paper of Asakura and Oosawa [6], where expression Eq. (3.1) was first derived, the polymers were regarded as (dilute) pure hard spheres. Vrij [5, 11] arrived at the same result by describing the polymer chains as penetrable hard spheres, see Sect. 3.2.

In a mixture of hard spheres and depletants (which can also be polymers, surfactant micelles, rodlike colloidal particles) a phase transition occurs upon exceeding a certain concentration of colloidal spheres and/or depletants. An important parameter that is used to describe the phase stability of colloid-polymer mixtures is the size ratio q,

$$q = \frac{R_g}{R}. \tag{3.3}$$

Phase diagrams of colloid-polymer mixtures are often described in terms of the volume fraction of colloids η and the *relative* polymer concentration:

$$\phi_p = \frac{n_b}{n_b^*} = \frac{\varphi}{\varphi^*}, \tag{3.4}$$

which is unity at the overlap concentration and can be regarded as the 'coil volume fraction' of polymer coils, exceeding unity in the semidilute concentration regime

and beyond.[1] Commonly ϕ_p is used as the parameter for 'polymer concentration'. The overlap concentration in kg/m^3 or g/L equals

$$\frac{3M_p}{4\pi R_g^3 N_{\text{av}}}, \tag{3.5}$$

where M_p is the molar mass of the polymer and N_{av} is Avogadro's number. The osmotic pressure Π in Eq. (3.1) can, using Eq. (3.4), be rewritten as $\Pi v_p/k_BT = \phi_p$. This allows to write the depletion interaction for spheres that touch, $W_{\text{dep}}(h = 0) = W_{\text{dep}}$ as:

$$\frac{W_{\text{dep}}}{k_BT} = -\phi_p\left(1 + \frac{3}{2q}\right) \quad , \tag{3.6}$$

which for small q boils down to $W_{\text{dep}} = -(3/2q)k_BT\phi_p$. This clarifies that at given ϕ_p the depletion force is very strong for small q.

Next a few examples are discussed where the effects of depletion were already noted long before Asakura and Oosawa rationalized the attractive interaction caused by depletants.

3.1.3 Early Observations

The aggregation of red blood cells (RBCs) in blood of human beings is found to be enhanced in case of for instance pregnancy or a wide range of illnesses, giving rather pronounced 'rouleaux'; clustered RBCs with their flat sides facing each other [12]. Rouleaux were described already more than 2 centuries ago. Enhanced RBC aggregation is observed for instance by measuring the sedimentation rate which can increase 100-fold in case of severe illnesses as compared to RBC sedimentation in healthy blood. The blood sedimentation test, based on monitoring aggregation of red blood cells, became a standard method for detecting illnesses. The relation between pathological condition, RBC aggregation and enhanced sedimentation rate was described for instance long time ago in [12–14]. It has been shown that adding macromolecules such as dextrans to blood also promotes rouleaux formation. Asakura and Oosawa [6] suggested that RBC aggregation is caused by depletion forces between the RBC's induced by serum proteins. The general picture is that

[1]The quantity n_b^* is the bulk polymer number density at which the polymer coils overlap. In terms of the volume fraction of polymer segments φ ($0 \leq \varphi \leq 1$), one then uses $\phi_p = \varphi/\varphi^*$, with φ^* the segment volume fraction at which the chains start to overlap: $\varphi^* = N_p v_s/v_p$, where N_p is the number of segments per polymer chain, v_s is the monomer (segment) volume, and $v_p = (4\pi/3)R_g^3$ the coil volume, so $\varphi^* \sim N_p/R_g^3$. The overlap number density n_b^* hence follows as $n_b^* = 3/(4\pi R_g^3)$.

red blood cells tend to cluster at elevated concentrations of the blood serum proteins, which act as depletants.

Large scale production of binder particles for paint production commenced about a century ago. In order to lower transport costs there was a significant interest in concentrating the polymeric latex. Centrifugation is highly energy consuming and thus expensive. Traube [15] showed that adding plant and seaweed polysaccharides led to a phase separation between a dilute and a concentrated phase with binder particles. Since the particles are lighter than the solvent the concentrated phase, with volume fraction $0.5 \leq \eta \leq 0.8$, floats on top. The lower phase is clear and hardly contains particles. Baker [16] and Vester [17] systematically investigated the mechanism that leads to what they called (enhanced) creaming. From the work of Baker [16] it can be concluded that the particles aggregate reversibly; upon dilution the latex particles can be resuspended. This suggests that bridging, which can also cause creaming [18], is not the driving force for enhanced creaming here.

3.1.4 Onset of Attention for Depletion After 1954

Not long after the publication of the work of Asakura and Oosawa, Sieglaff [19] demonstrated that a depletion-induced phase transition may occur upon adding polystyrene to a dispersion of microgel spheres in toluene. This demonstrated that the attractive depletion force is sufficiently strong to induce a phase separation. Sieglaff rationalized his findings in terms of the theory of Asakura and Oosawa. It took more than a decade before subsequent work was published.

Early systematic studies with respect to phase stability for colloid-polymer mixtures were performed in the 1970s by Vincent and co-workers [7, 20, 21]. They concentrated on mixtures of colloidal spheres (latex particles) plus nonadsorbing polymers such as polyethylene oxide (PEO). In the papers of Vincent et al. there is quite some variation in qualifying the demixing phenomena in colloid-polymer mixtures [20, 22–24]. These experiments were ahead of a full theoretical understanding of the phase behaviour of colloid-polymer mixtures.

Also in the 1970s Hachisu et al. [25] investigated aqueous dispersions of negatively charged polystyrene latex particles that undergo a colloidal fluid-to-solid phase transition upon lowering the salt concentration using dialysis or increasing the particle concentration. Under conditions where the latex dispersion is not ordered (fluid-like), Kose and Hachisu [26] added sodium polyacrylate to polystyrene latex particles (both components are negatively charged), and observed crystallization of the colloidal spheres. The authors suggested that the ordering is due to ‘some attractive force’. When the polymer concentration is increased crystallization occurs faster. Since polymers and particles repel each other the crystallization process was probably induced by depletion interaction.

Theoretical work on depletion interactions and their effects on macroscopic properties such as phase stability started with work by Vrij [5] who considered the depletion interaction between hard spheres due to dilute nonadsorbing polymers

described as penetrable hard spheres (see Sect. 3.2) and computed the second osmotic virial coefficient to explain the phase transitions observed by De Hek and Vrij [11]. By mixing aqueous hydroxyethylcellulose (HEC) with polymeric colloidal particles, Sperry [27, 28] and coworkers [29] observed phase separation and made a study on the effect of the structure of the colloid-rich phase as a function of the colloidal particle-free polymer size ratio $q = R_g/R$. Unstable systems at large q and not too high polymer concentrations are characterized by smooth interfaces, implying colloidal gas–liquid coexistence. For small q, demixed systems are characterized by irregular interfaces that indicate (colloidal) fluid-solid coexistence. This suggests that the width of the region where a colloidal liquid is found in colloid-polymer mixtures is limited.

The work of Sperry inspired Gast, Hall and Russel to develop a theory which might explain the experimental phenomena. Gast et al. [30] used thermodynamic perturbation theory (TPT) [31] to derive the free energy of a mixture of colloidal particles and polymers (described as phs; penetrable hard spheres), based on pair-wise additivity of the interactions between the colloids. They calculated the phase behaviour from the (perturbed) free energy which made it possible to assign the nature (i.e. colloidal gas, liquid or solid) of the coexisting phases as a function of size ratio q, the concentration (or formally activity within their approach) of the polymers, and the volume fraction of colloids. For small values of q, say, $q = R_g/R < 0.3$, increasing the polymer concentration broadens the hard sphere fluid-solid coexistence region; a (stable) colloidal fluid-solid coexistence is expected if the polymer chains are significantly smaller than the colloidal spheres (low q). Inside the unstable regions a (metastable) colloidal gas–liquid branch is located. For intermediate values of q, the gas–liquid coexistence curve crosses the fluid-solid curve and for large q-values mainly gas–liquid coexistence is found for $\eta < 0.49$, where η is the volume fraction of colloids. The results are in agreement with the findings of Sperry [27–29]. Experimentally, Gast et al. [32] later verified the predicted types of phase coexistence regions for a model colloid-polymer system. Colloid-polymer phase diagrams are commonly plotted in terms of the volume fraction of colloids η and the *relative* polymer concentration ϕ_p, defined in Eq. (3.4).

A semigrand canonical treatment for the phase behaviour of colloidal spheres plus nonadsorbing polymers was proposed by Lekkerkerker [33], who developed 'free volume theory' (also called 'osmotic equilibrium theory'), see Sect. 3.3.4. The main difference with TPT [30] is that free volume theory (FVT) accounts for polymer partitioning between the phases and corrects for multiple overlap of depletion layers, hence avoids the assumption of pair-wise additivity which becomes inaccurate for relatively thick depletion layers. These effects are incorporated through scaled particle theory (see for instance [34] and references therein). The resulting free volume theory (FVT) phase diagrams calculated by Lekkerkerker et al. [35] revealed that for $q < 0.3$ coexisting fluid-solid phases are predicted, whereas at low colloid volume fractions a gas–liquid coexistence is found for $q > 0.3$, as was predicted by TPT. A coexisting *three*-phase colloidal gas–

liquid-solid region, not present in TPT phase diagrams, was predicted by FVT for $q > 0.3$ and gained much attention. Experimental work [36, 37] demonstrated that this three-phase region indeed exists. Before the basics of phase behaviour of colloidal dispersions are discussed in more detail the focus is now first on the depletion interaction where more detailed derivations of the basic results are provided.

3.2 Depletion Interaction

In this section the depletion interaction between two flat plates and between two spherical colloidal particles is considered for penetrable hard spheres (phs). It is noted that besides polymers (for which PHS are a reasonable model when the polymers are small and dilute), small colloidal spheres, rods and plates can also act as depletants, see [38]. The penetrable hard sphere model, implicitly introduced by Asakura and Oosawa [2] and considered explicitly in detail by Vrij [5], is characterized by the fact that the spheres freely overlap each other but act as hard spheres with diameter 2δ when interacting with a wall or a colloidal particle.

3.2.1 Depletion Interaction Between Two Flat Plates

Consider Fig. 3.3 where two parallel flat plates in a polymer solution are sketched. The force per unit area, $K(h)$, between two parallel plates separated by a distance h,

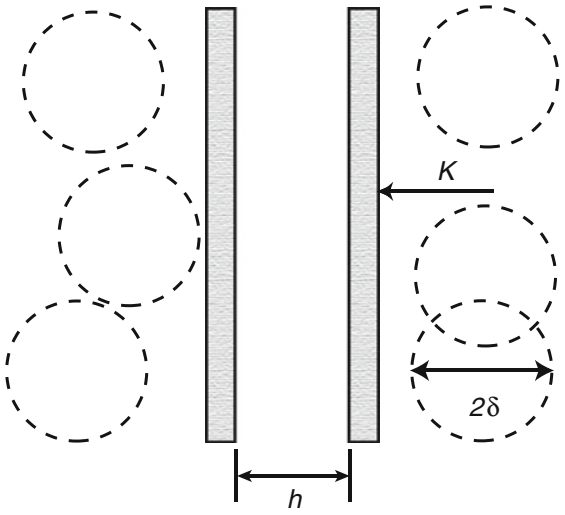

Fig. 3.3 Schematic picture of two *parallel flat plates* in the presence of penetrable hard spheres (*dashed circles*)

is the difference between the osmotic pressure Π_i inside the plates and the outside pressure Π_o

$$K = \Pi_i - \Pi_o. \tag{3.7}$$

Since the penetrable hard spheres behave thermodynamically ideally the osmotic pressure outside the plates is given by the Van 't Hoff law $\Pi_o = n_b k_B T$, where n_b is the bulk number density of the phs. When the plate separation h is equal to or larger than the diameter $\sigma(= 2\delta)$ of the penetrable hard spheres the osmotic pressure inside the plates is the same as outside, $\Pi_i = \Pi_o = n_b k_B T$. On the other hand, when the plate separation is less than the diameter of the penetrable hard spheres, no particles can enter the gap and $\Pi_i = 0$. This means that

$$K(h) = \begin{cases} -n_b k_B T & 0 \le h < 2\delta \\ 0 & h > 2\delta \end{cases}. \tag{3.8}$$

Since $K = -\mathrm{d}W/\mathrm{d}h$, integration yields the interaction potential $W(h)$ per unit area $W(h)$ between the plates

$$W(h) = \begin{cases} -n_b k_B T(2\delta - h) & 0 \le h < 2\delta \\ 0 & h \ge 2\delta \end{cases}. \tag{3.9}$$

3.2.2 Depletion Interaction Between Two Spheres

When the depletion zones with thickness δ around spherical colloidal particles with radius R start to overlap, i.e., when the distance $r(= h + 2R)$ between the centers of the colloidal particles is smaller than $2R + 2\delta$, a net force arises between the colloidal particles. It is useful to define an effective depletion radius R_d:

$$R_d = R + \delta. \tag{3.10}$$

The (attractive) force originates from an uncompensated (osmotic) pressure due to the depletion of penetrable hard spheres from the gap between the colloidal spheres. This is illustrated in Fig. 3.4 from which it can be deduced that the uncompensated osmotic pressure acts on the surface between $\theta = 0$ and $\theta_0 = \arccos(r/2R_d)$. For obvious symmetry reasons only the component along the line connecting the centers of the colloidal spheres contributes to the total force. For the angle θ this component is $\Pi_o \cos\theta$ where the pressure is $\Pi_o = n_b k_B T$. The surface on which this force acts between θ and $\theta + \mathrm{d}\theta$ equals $2\pi R_d^2 \sin\theta \mathrm{d}\theta$. The total force between the colloidal spheres is obtained by integration:

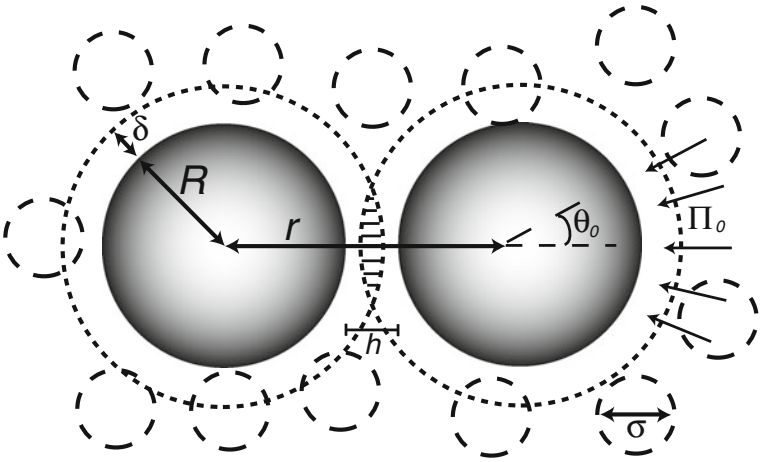

Fig. 3.4 Two hard spheres in the presence of penetrable hard spheres as depletants. The PHS impose an unbalanced osmotic pressure Π between the hard spheres resulting in an attractive force between them. The overlap volume of depletion layers between the hard spheres (*hatched*) has the shape of a lens with width $2\delta - h$ and height $2H = 2R_d \sin\theta_0$, where θ_0 is given by $\cos\theta_0 = r/2R_d$

$$K_s(r) = -2\pi n_b k_B T (R+\delta)^2 \int_0^{\theta_0} \sin\theta\cos\theta \, \mathrm{d}\theta. \tag{3.11}$$

Hence

$$\frac{K_s(r)}{n_b k_B T} = \begin{cases} \infty & r < 2R \\ -\pi R_d^2 [1 - (r/2R_d)^2] & 2R \le r \le 2R_d \\ 0 & r > 2R_d \end{cases}. \tag{3.12}$$

The minus sign in the right-hand side of Eq. (3.12) implies that the force is attractive. The depletion potential is now obtained by integration of the depletion force Eq. (3.12)

$$\begin{aligned} W_s(r) &= \int_r^{2R_d} K_s(r)\mathrm{d}r \\ &= \infty \qquad\qquad r < 2R \\ &= -n_b k_B T V_{ov}(r) \quad 2R \le r \le 2R_d \\ &= 0 \qquad\qquad r > 2R_d \end{aligned}, \tag{3.13}$$

with

$$V_{ov}(r) = \frac{4\pi}{3} R_d^3 \left[1 - \frac{3}{4}\frac{r}{R_d} + \frac{1}{16}\left(\frac{r}{R_d}\right)^3 \right] \tag{3.14a}$$

$$V_{\rm ov}(h) = \frac{\pi}{6}(2\delta - h)^2(3R + 2\delta + h/2) \tag{3.14b}$$

The result of Eq. (3.14a), in which r is the variable, was first obtained by Vrij [5] with PHS explicitly as depletants. In Eq. (3.14b) the variable is h and was already given (without explicit derivation) in Eq. (3.2). Both Eqs. (3.14a) and (3.14b) are frequently used in the literature.[2] The expression for $W_{\rm s}(r)$ in Eq. (3.13) equals the osmotic pressure ($n_b k_B T$) times overlap volume $V_{\rm ov}$. In the (Derjaguin) limit $\delta \ll R$ the attractive parts of the force (Eq. 3.11) and interaction potential (Eq. 3.13) between the spheres take on even simpler forms:

$$\frac{K_{\rm s}(h)}{n_b k_B T} = -\pi R(2\delta - h) \tag{3.15}$$

and

$$\frac{W_{\rm s}(h)}{n_b k_B T} = -2\pi R(\delta - h/2)^2. \tag{3.16}$$

For the contact potential $W_{\rm dep} = W_{\rm s}(h = 0)$ the result

$$\frac{W_{\rm dep}}{k_B T} = -2n_b \pi R\delta^2 = -\frac{3}{2}\frac{\phi_d}{q} \tag{3.17}$$

is obtained, where ϕ_d is the relative concentration of penetrable hard spheres $4\pi\delta^3 n_b/3$, see also the definition of Eq. (3.4) for ϕ_p.

It is noted that in case of (small) hard spheres as depletants the results are identical to those above only in the dilute limit. For the minimum attraction between two spheres at contact the depletion force up to second order in hard sphere depletant volume fraction η_{ss} is [38, 39]:

$$\frac{W_{\rm s,min}}{k_B T} = -\frac{3}{2}\frac{R}{\delta}\left(\eta_{ss} + \frac{1}{5}\eta_{ss}^2\right), \tag{3.18}$$

where δ now equals the radius of the small hard spheres. For small values of η_{ss} Eq. (3.17) is recovered for $\eta_{ss} = \phi_d$. At higher volume fractions the depletion attraction at contact between the big hard spheres by small hard spheres is however larger than the depletion due to penetrable hard spheres. Besides a depletion

[2] A smooth transition between these forms is:

$$V_{\rm ov}(r) = \frac{2\pi}{3}(R_d - r/2)^2(2R_d + r/2).$$

.

attraction, depletion effects of small hard spheres also lead to a repulsive contribution to the interaction between two spheres. Near $h = 2\delta$ a positive maximum of the pair interaction is found with a maximum (up to second order in η_{ss})

$$\frac{W_{\mathrm{s,max}}}{k_B T} = \frac{6R}{5\delta}\eta_{ss}^2.$$

3.3 Phase Behaviour of Colloidal Dispersions

Phase transitions are the result of physical properties of a collection of particles depending on the colligative properties. In Sect. 3.2 we focused on two-body interactions. Depletion effects are commonly not pair-wise additive [40–43]. Therefore, the prediction of phase transitions of particles with depletion interaction is not straightforward. As a starting point the Van der Waals model is recalled and applied to a collection of colloidal spheres with long-ranged attraction. Then a more advanced description for the thermodynamic properties of the pure colloidal dispersion are given. Subsequently, this is used to describe the phase behaviour of a collection of hard spheres plus additional Yukawa attraction, with a variable range of the interaction. Next, the basics of the free volume theory for the phase behaviour of colloids + depletants is explained. Only the simplest type of depletant, the penetrable hard sphere, is considered here. For experimental methods that enable measuring (depletion) interaction potentials between particles I refer to [44].

3.3.1 Phase Behaviour of a Van der Waals Fluid

The seminal equation of state of van der Waals [45] for the pressure P for N particles in a volume V reads:

$$P = \frac{Nk_B T}{V - bN} - a\left(\frac{N}{V}\right)^2. \tag{3.19}$$

Here b is the excluded volume per particle, which is $4v_c$ for hard spheres. Using this equation van der Waals could implicitly demonstrate that a fluid can only phase separate when there is both excluded volume interaction (expressed via the contribution of the bN term) as well as attraction (the aN^2/V^2 term) between the molecules. It allows to describe the gas–liquid equilibria for a wide range of atomic and molecular substances and it revealed that the phase behaviour of low molecular systems is rather universal.

Let us now describe a colloidal dispersion of hard spheres plus an attraction in a very simple manner using the van der Waals model of Eq. (3.19). This can be done

when considering the solvent in a colloidal dispersion as effective background. When performing computations on phase coexistence it is useful to use normalized quantities. Hence the normalized Helmholtz energy $\widetilde{F}$, the dimensionless chemical potential $\tilde{\mu}$ and normalized pressure $\widetilde{\Pi}$ are introduced:

$$\begin{aligned} \widetilde{F} &= \frac{F v_c}{k_B T V}, \quad \tilde{\mu} = \frac{\mu}{k_B T} \\ \eta &= \frac{N v_c}{V}, \quad \widetilde{\Pi} = \frac{\Pi v_c}{k_B T}. \end{aligned} \tag{3.20}$$

For sake of completeness the definition of the volume fraction η is added. Note that instead of the pressure P of a molecular fluid here the normalized *osmotic* pressure Π is used because solvent is present.

The van der Waals equation can now be rewritten in dimensionless form:

$$\widetilde{\Pi} = \frac{\eta}{1-4\eta} - \gamma\eta^2, \tag{3.21}$$

with $\gamma = a/(k_B T v_c)$. In order to compute phase coexistence the osmotic pressure and the chemical potential for the van der Waals fluid are required. From thermodynamics ($P = -(\partial F/\partial V)_{N,T}$) it follows

$$\widetilde{\Pi} = -\left(\frac{\partial(\widetilde{F}/\eta)}{\partial(1/\eta)}\right)_{V,T} = \eta\left(\frac{\partial\widetilde{F}}{\partial\eta}\right)_{V,T} - \widetilde{F} = \eta\tilde{\mu} - \widetilde{F}. \tag{3.22}$$

Hence the Helmholtz energy follows as:

$$\widetilde{F} = \eta\ln(\Lambda^3/v_c) + \eta\ln\eta - \eta - \eta\ln(1-4\eta) - \gamma\eta^2. \tag{3.23}$$

The last two terms are the result of the integration of Eq. (3.21) using Eq. (3.22). The other terms are the ideal contributions that follow from the ideal gas reference state [46]; Λ is the De Broglie wavelength.[3] Using

$$\tilde{\mu} = \left(\frac{\partial\widetilde{F}}{\partial\eta}\right)_{N,T}, \tag{3.24}$$

the chemical potential follows as

$$\tilde{\mu} = \tilde{\mu}^{+} + \ln\left(\frac{\eta}{1-4\eta}\right) + \frac{4\eta}{1-4\eta} - 2\gamma\eta, \tag{3.25}$$

[3] $\Lambda = h/\sqrt{2\pi m_c k_B T}$, with the colloid mass m_c and Planck's constant h.

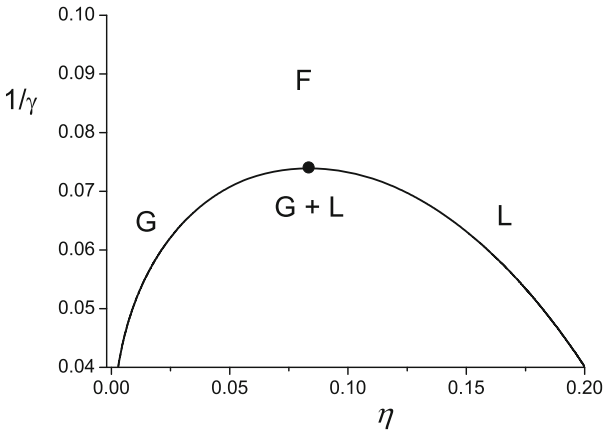

Fig. 3.5 Gas–liquid binodal following the van der Waals equation of state. The full *circle* is the critical point

with $\tilde{\mu}^{+} = \ln \Lambda^3 / v_c$. Now all ingredients to compute gas–liquid coexistence are available. The binodal gas–liquid coexistence curve follows from solving the coexistence conditions

$$\begin{aligned} \widetilde{\Pi}(\eta_G) &= \widetilde{\Pi}(\eta_L) \\ \tilde{\mu}(\eta_G) &= \tilde{\mu}(\eta_L) \end{aligned}, \tag{3.26}$$

where η_G and η_L are the volume fractions of the particles in the gas and liquid phases, respectively. In Fig. 3.5 the binodal is plotted. The critical point (cp) follows analytically from Eq. 3.21 as $\gamma_{cp} = 27/2$ and $\eta_{cp} = 1/12$ and is indicated as full circle. The quantity γ^{-1} can be regarded as effective temperature. It is clear from Eq. (3.21) that the description of the fluid diverges at $\eta = 0.25$, which is in fact incorrect. Therefore the focus is first on more accurate expressions for the equations of state for a collection of pure hard spheres in the next section.

3.3.2 Phase Behaviour of a Hard Sphere Dispersion

The focus is first on the equation of state for the fluid phase of hard spheres interacting through the hard-sphere interaction

$$W(h) = \begin{cases} \infty & \text{for} \quad h < 0 \\ 0 & \text{otherwise} \end{cases}, \tag{3.27}$$

Carnahan and Starling [48] found that the second and higher order virial coefficients for a collection of hard spheres can, to a good approximation, can be written as

Table 3.1 Values for the 2nd up to the 8th virial coefficient of hard spheres [47] in comparison with the Carnahan-Starling result Eq. (3.28). The numbers in the second and third column are B_i/v_c^{i-1} for $i = 2, 3, \ldots 0.8$

i	Exact/Numerical	CS Eq. (3.28)
2	4	4
3	10	10
4	18.36	18
5	28.22	28
6	39.82	40
7	53.34	54
8	68.53	70

$$B_{m+1} = (m^2 + 3m)v_c^m. \tag{3.28}$$

In Table 3.1 exact [47] virial coefficients are compared with the approximation given by Eq. (3.28). Inserting Eq. (3.28) into the general definition for the virial expansion of the (osmotic) pressure[4] [49],

$$\frac{\Pi_f^0 v_c}{k_B T} = \eta + \sum_{m=2} \frac{B_m}{v_c^{m-1}} \eta^m, \tag{3.29}$$

yields the Carnahan-Starling equation of state [48] for a fluid of (colloidal) hard spheres:

$$\widetilde{\Pi}_f^0 = \frac{\Pi_f^0 v_c}{k_B T} = \frac{\eta + \eta^2 + \eta^3 - \eta^4}{(1-\eta)^3}. \tag{3.30}$$

In Fig. 3.6 (left part) the (osmotic) pressure given by the Carnahan-Starling equation of state is compared to computer simulation data. Obviously, Eq. (3.30) is indeed very accurate.

From the Gibbs-Duhem relation $S\mathrm{d}T - V\mathrm{d}\Pi + N\mathrm{d}\mu = 0$ the chemical potential can be calculated from the pressure. For constant T this relation may be written as

$$\mathrm{d}\Pi = \frac{\eta}{v_c}\mathrm{d}\mu. \tag{3.31}$$

Now μ follows as

$$\mu = k_B T \ln \frac{\Lambda^3}{v_c} + v_c \int_0^\eta \frac{1}{\eta'} \frac{\mathrm{d}\Pi}{\mathrm{d}\eta'} \mathrm{d}\eta', \tag{3.32}$$

where $\mathrm{d}\Pi/\mathrm{d}\eta$ can be calculated from Eq. (3.30) for a fluid of hard spheres. The result for the chemical potential (normalized as $\tilde{\mu} = \mu/k_B T$) of a hard sphere in a fluid with volume fraction of hard spheres η follows now as

[4] the '0' refers to hard spheres and the subscript 'f' indicates a fluid phase.

$$\tilde{\mu}_f^0 = \ln\frac{\Lambda^3}{v_c} + \ln\eta + \frac{3-\eta}{(1-\eta)^3} - 3 \tag{3.33}$$

Using the standard thermodynamic result $\widetilde{\Pi} = \eta\tilde{\mu} - \widetilde{F}$, the resulting canonical free energy of the pure hard-sphere dispersion of a fluid is:

$$\widetilde{F}_f^0 = \eta\left[\ln(\eta\Lambda^3/v_c) - 1\right] + \frac{4\eta^2 - 3\eta^3}{(1-\eta)^2}. \tag{3.34}$$

The first term on the right-hand side of Eq. (3.34) is the ideal contribution, while the second hard-sphere interaction term is the Carnahan-Starling equation of state [48].

To obtain the thermodynamic functions of the hard-sphere crystal one can use the cell model of Lennard-Jones and Devonshire [52]. For details I refer to our book [38]. The cell model result for the normalized Helmholtz energy of an fcc crystal is

$$\widetilde{F}_s^0 = \eta\ln\left(\frac{27\Lambda^3}{8v_c}\right) - 3\eta\ln\left[\frac{\eta_{cp}}{\eta} - 1\right], \tag{3.35}$$

where $\eta_{cp} = \pi/3\sqrt{2} \simeq 0.74$ is the volume fraction at close packing. Using Eqs. (3.22) and (3.24) the dimensionless osmotic pressure and chemical potential become:

$$\widetilde{\Pi}_s^0 = \frac{3\eta}{1-\eta/\eta_{cp}}, \tag{3.36}$$

and

$$\tilde{\mu}_s^0 = \ln\frac{\Lambda^3}{v_c} + \ln\left[\frac{27}{8\eta_{cp}^3}\right] + 3\ln\left[\frac{\eta}{1-\eta/\eta_{cp}}\right] + \frac{3}{1-\eta/\eta_{cp}}. \tag{3.37}$$

The pressure given by Eq. (3.36) can be compared to computer simulation data and, as can be seen in Fig. 3.6 (right part), turns out to be highly accurate. The result for the chemical potential given by Eq. (3.37) is close to the computer simulation results. The constant on the right-hand side $\ln\left[27/8\eta_{cp}^3\right] = 2.1178$ is quite close to 2.1306, which can be abstracted from computer simulations [53]. The full free energy expression for the hard-sphere solid phase can now also be written as

$$\widetilde{F} = 2.1178\,\eta + 3\,\eta\ln\left(\frac{\eta}{1-\eta/\eta_{cp}}\right) + \eta\ln\left(\Lambda^3/v_c\right). \tag{3.38}$$

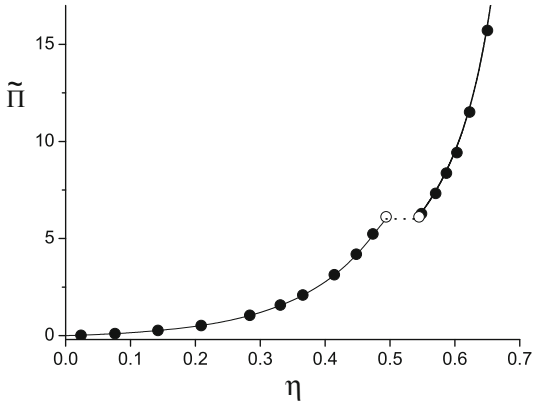

Fig. 3.6 The (*osmotic*) pressure of hard spheres. The *curves* are the Carnahan-Starling expression Eq. (3.30) for a fluid ($\eta \leq 0.494$) and the cell model result Eq. (3.36) for an fcc crystal (*solid curves*; $\eta \geq 0.545$). The full symbols are Monte Carlo computer simulation results [50]. The two *open symbols* correspond to the fluid-solid coexistence from simulation [51], the *dotted line* connects these binodal points

Solving the coexistence conditions

$$\begin{aligned} \widetilde{\Pi}_f^0(\eta_f) &= \widetilde{\Pi}_s^0(\eta_s) \\ \tilde{\mu}_f^0(\eta_f) &= \tilde{\mu}_s^0(\eta_s) \end{aligned}, \tag{3.39}$$

yields coexisting volume fractions $\eta_f = 0.491$, $\eta_s = 0.541$ and a coexistence pressure $\widetilde{\Pi} = 6.01$. These values are indeed very close to computer simulation results, first accurately performed by Hoover and Ree [51], see the comparison in Fig. 3.6.

A collection of pure hard spheres is athermal; the thermodynamic properties are fully determined by entropy. At low densities the configurations of maximum entropy correspond to disordered arrangements. As the density increases crystalline arrangements lead to a more efficient packing and make more arrangements possible above some volume fraction, see Fig. 3.7. The fluid–crystal transition has been observed for instance in suspensions of sterically stabilized silica particles [54] and sterically stabilized PMMA particles [55] with low size dispersity. In addition to the fluid-crystal transition an amorphous glassy phase was observed above a volume fraction $\eta = 0.58$. For such high volume fractions the particles become so tightly trapped or caged that they do not crystallize but remain in long-lived metastable states, termed called colloidal glasses.

Accurate expressions for the equation of state of a fluid of hard spheres and for an fcc crystal of hard spheres have been presented above and will be used further on. Next it is interesting to account for additional attractions between the particles. As Boltzmann already pointed out [56] the attractive term of the van der Waals equation is only valid for long-ranged attractions. In order to investigate the effect

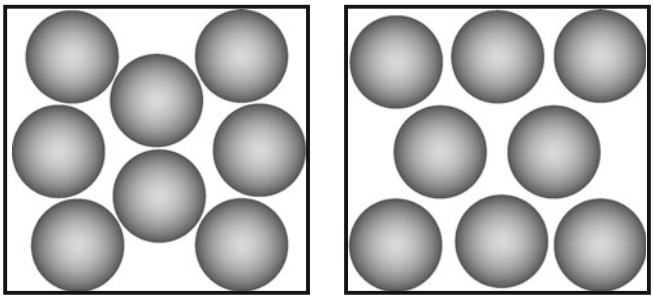

Fig. 3.7 Schematic pictures of a hard-sphere fluid (*left*) and hard spheres with 'crystalline' order (*right*); free volume entropy drives freezing

of the range of the attraction on the phase behaviour the focus is therefore now on particles with a hard-core plus Yukawa[5] attraction.

3.3.3 Phase Behaviour of a Dispersion of Hard Cores Plus Yukawa Attraction

Here a collection of hard-core spheres with hard-core diameter $2R$ plus a Yukawa attraction is considered. The hard-core Yukawa pair potential between two spheres can be written as[6]

$$W(h) = \begin{cases} \infty & \text{for} \quad h<0 \\ -\frac{\varepsilon}{1+h/2R}\exp(-\kappa h) & \text{otherwise} \end{cases}, \tag{3.40}$$

where h equals $r-2R$, with r the centre-to-centre distance. The strength of the attraction is the contact potential $W(0)=\varepsilon$ and the range is the screening length κ^{-1}. The relative range of attraction q_Y (with respect to the particle radius R) is defined as $1/\kappa R$.

For a collection of particles interacting through this pair interaction it is possible to derive an equation of state. Tang and Lu [57] solved the Ornstein-Zernicke (OZ) equation using the mean spherical approximation (MSA) closure in Fourier and Laplace space and found that each perturbation term in the contact potential can be solved analytically. For the first-order expansion, termed FMSA, this leads to relatively simple and rather accurate solutions for the thermodynamic properties [58, 59].

[5]The term Yukawa potential originally stems stems from the quantum mechanical theory of nuclear interactions. In a more general context, it is often used for potentials with a distance profile of the type $\exp\{-\kappa r\}/r$.

[6]Although here only Yukawa attractions are considered this description also holds for spheres interacting through a hard-core repulsive Yukawa interaction.

Tang et al. [59] derived an analytical expression for $\widetilde{F}$ (see Fig. 3.8 for an illustration of determining coexistence points from the free energy) that is accurate and which can be written in the Van der Waals-form, albeit the γ term is now dependent on η ($G \sim \gamma\eta^2$). Tuinier and Fleer [60] found that this form can be simplified even more with almost no loss of accuracy. The final form is

$$\widetilde{F} = \widetilde{F}^0 - \beta\varepsilon G(\eta), \tag{3.41}$$

where $\beta = 1/k_BT$ with a simple volume fraction-dependent function $G(\eta)$,

$$G(\eta) = \eta^2 \frac{a_0 + a_1\eta}{b_0 + b_1\eta + b_2\eta^2}. \tag{3.42}$$

The coefficients a_i and b_i depend only on the relative range of the Yukawa potential q_Y. They are expressed most easily in its inverse $k = 1/q_Y = \kappa R$:

$$\begin{aligned} a_0 &= 4k^2 + 2k \\ a_1 &= 2k^2 + 4k \end{aligned} \tag{3.43}$$

and

$$\begin{aligned} b_0 &= \frac{2k^3}{3} \\ b_1 &= \chi_1 - \frac{4k^3}{3} + 2k^2 - 1 \\ b_2 &= \chi_2 + \frac{2k^3}{3} - 2k^2 + 3k - 2, \end{aligned} \tag{3.44}$$

where χ_1 and χ_2 are defined as:

$$\begin{aligned} \chi_1 &= (2k+1)\exp(-2k) \\ \chi_2 &= (k+2)\exp(-2k). \end{aligned} \tag{3.45}$$

Note that a volume fraction-independent γ survives in the low η-limit, for which G becomes $3q_Y(2+q_Y)\eta^2$, so $\gamma = -3\beta\varepsilon q_Y(2+q_Y)$.[7] However, in very concentrated systems G becomes proportional to η.

An analytical expression for the chemical potential is obtained from $\tilde{\mu} = \partial\tilde{F}/\partial\eta$:

$$\tilde{\mu} = \tilde{\mu}^0 - \beta\varepsilon H(\eta), \tag{3.46}$$

[7]This can be regarded as an explicit definition for γ within the van der Waals model when the attraction is described as a long-ranged Yukawa attraction.

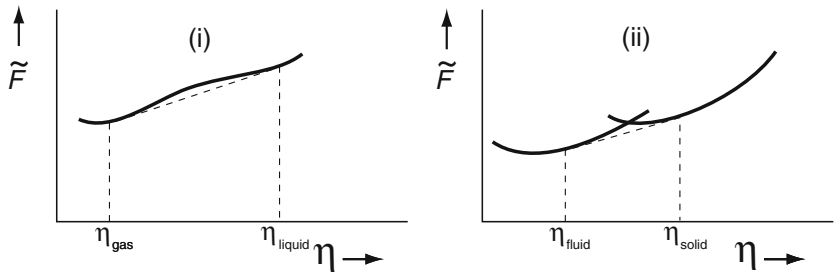

Fig. 3.8 The dimensionless Helmholtz energy $\widetilde{F} = \eta\tilde{\mu} - \widetilde{\Pi}$ as a function of volume fraction η. Schematic view of the common tangent construction (*straight lines*) to determine the phase coexistence in mixtures of colloidal hard spheres and phs. (i): gas–liquid coexistence, (ii): fluid-solid coexistence. The *dashed lines* represent the common tangent construction with intercept $-\widetilde{\Pi}$ and *slope* $\tilde{\mu}$

where $H(\eta)$ is given by:

$$H(\eta) \;=\; k\eta\frac{c_0 \;+\; c_1\eta \;+\; c_2\eta^2 \;+\; c_3\eta^3}{\left(b_0 \;+\; b_1\eta \;+\; b_2\eta^2\right)^2}, \tag{3.47}$$

with the following q-dependent coefficients:

$$\begin{aligned}
c_0 &= \frac{8k^4}{3} + \frac{4k^3}{3} \\
c_1 &= (2k+1)\chi_1 + \frac{8k^4}{3} + \frac{14k^3}{3} + 3k^2 + 2k + 1 \\
c_2 &= (k+2)\chi_1 - \frac{4k^4}{3} - \frac{2k^3}{3} + 4k^2 + k + 1 \\
c_3 &= (2k+1)\chi_2 + \frac{4k^4}{3} - \frac{10k^3}{3} + 4k^2 - 3k - 2
\end{aligned} \tag{3.48}$$

The (osmotic) pressure follows from $\widetilde{\Pi} = \eta\tilde{\mu} - \widetilde{F}$:

$$\widetilde{\Pi} \;=\; \widetilde{\Pi}^0 \;+\; \beta\varepsilon J(\eta), \tag{3.49}$$

with $J(\eta)$ given by:

$$J(\eta) \;=\; G(\eta) - \eta H(\eta). \tag{3.50}$$

Now analytical expressions are available for both $\tilde{\mu}$ and $\widetilde{\Pi}$.

In principle this provides sufficient information to compute the binodal curves. In Fig. 3.9 gas–liquid binodals for attractive hard core Yukawa spheres are plotted for various ranges of the attraction κR. As an illustration computer simulation results are plotted as data points as well. It is clear that the unstable region shifts to

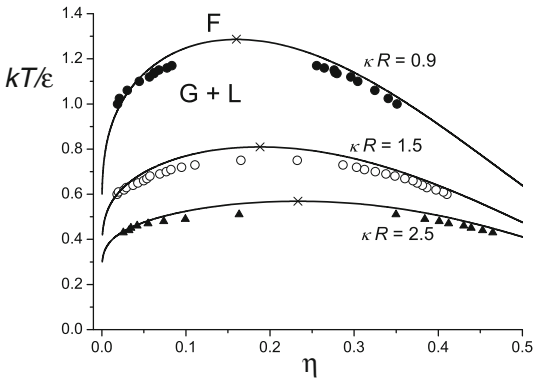

Fig. 3.9 Gas–liquid coexistences of a collection of hard-core attractive Yukawa spheres for three values of κR as indicated. Symbols are simulation results [61], the *solid curves* are the analytical expressions for the binodals. *Crosses* represent the theoretical critical points

lower temperatures for shorter ranges of attraction; at identical values of $k_BT/\varepsilon = \beta\varepsilon$ there is similar attraction at close contact between the spheres but there is an additional attraction when the spheres are further apart in case of smaller κR.

In order to calculate the gas–liquid binodal ε is eliminated from Eqs. (3.46) and (3.49) to find the analytical coexistence relation:

$$\beta\varepsilon = \frac{\tilde{\mu}_l^0(\eta_l) - \tilde{\mu}_g^0(\eta_g)}{H(\eta_l) - H(\eta_g)} = \frac{\widetilde{\Pi}_l^0(\eta_l) - \widetilde{\Pi}_g^0(\eta_g)}{J(\eta_g) - J(\eta_l)}. \tag{3.51}$$

For both μ_g^0 and μ_l^0 Eq. (3.33) is used and for both Π_g^0 and Π_l^0 Eq. (3.30) is applied. For a given q the second and third parts of this equation relate the volume fractions at coexistence. For instance, a value for η_g is chosen and the corresponding η_l is solved using the second equality of Eq. (3.51). The first equality then tells to which Yukawa contact potential ε those binodal concentrations correspond. It is noted that the calculation of binodals in the analytical model involve nothing more than solving one equation in one unknown.

Fluid–solid coexistence is obtained analogously:

$$\varepsilon = \frac{\mu_s^0(\eta_s) - \mu_f^0(\eta_f)}{H(\eta_s) - H(\eta_f)} = \frac{\Pi_s^0(\eta_s)v - \Pi_f^0(\eta_f)v}{J(\eta_f) - J(\eta_s)}. \tag{3.52}$$

In this case μ_s^0 is used from Eq. (3.37) and Π_s^0 from Eq. (3.36). As in Eq. (3.51), the fluid parts are obtained from Eqs. (3.30) and (3.33).

In Fig. 3.10 a full phase diagram (gas–liquid and fluid–solid) is presented for $\kappa R = 2$ and compared to computer simulation results. It follows that there is a region where there is a stable fluid (low η, high T), a region where the fluid phase separates into a gas and a liquid below the critical point, a region where fluid and solid coexist (near $0.45 \lesssim \eta \lesssim 0.6$), a region where there is a solid phase (high η) and a gas–solid coexistence region (low T).

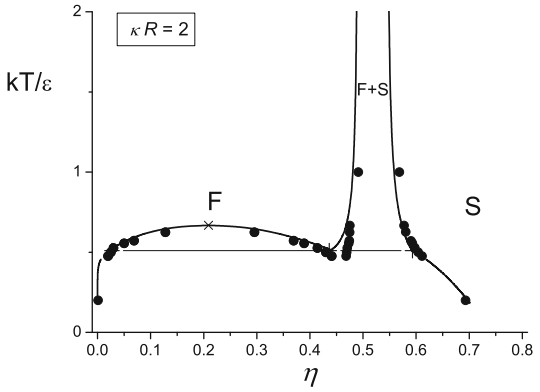

Fig. 3.10 Phase behavior of a dispersion of spherical hard-core attractive Yukawa particles with $\kappa R = 2$. Symbols are simulation results [62], the *solid curves* are the analytical results. *Cross* is the theoretical critical point, plusses identify the three coexisting phases of the triple points; the three plusses are connected through a *thin line*

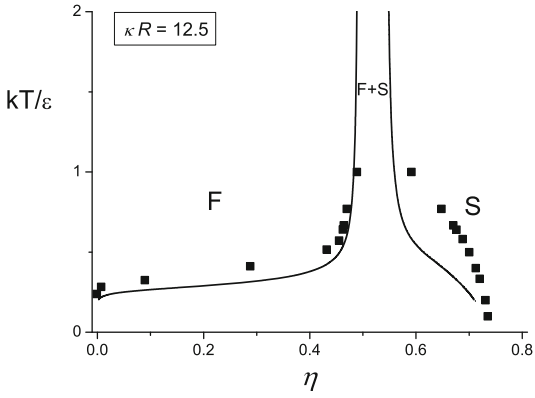

Fig. 3.11 As Fig. 3.10 but for $\kappa R = 12.5$. The GL coexistence is now metastable, and there is no triple point

For large values of κR the gas–liquid region becomes metastable with respect to fluid-solid coexistence. See Fig. 3.11 where the fluid-solid binodals are plotted for $\kappa R = 12.5$. Stable liquid configurations require that the particles still attract one another when their interparticle distance fluctuates. Hence for short-ranged attractions the gas–liquid coexistence gets metastable.

3.4 Phase Behaviour of a Colloid-Polymer Mixture

Several theories have been developed that enable calculations of phase transitions in systems with depletion interactions. The first successful treatment accounting for the colligative thermodynamic properties mediated by depletion interactions

[24, 30] is thermodynamic perturbation theory [46, 49]. In this classical approach depletion effects can be treated as a perturbation to the hard-sphere free energy, as was done by Gast et al. [30]. Their work predicted that for a sufficient depletant concentration, the depletion interaction leads to a phase diagram with stable colloidal gas, liquid and solid phases for $\delta/R \geq 0.3$. For small depletants with $\delta/R \leq 0.3$ only colloidal fluid and solid phases are thermodynamically stable, and the gas–liquid transition is meta-stable. Although implementation of this theory is straightforward, it has the drawback that it does not account for depletant partitioning over the coexisting phases. Subsequent developments originate from liquid state approaches. Examples are density functional theory [63], PRISM [64] and the Gaussian core model [65].

3.4.1 Free Volume Theory

In the early nineties of the last century a theory that accounts for depletant partitioning over the coexisting phases was developed [35], which nowadays is commonly referred to as free volume theory (FVT) [66]. This theory is based upon considering the osmotic equilibrium between a (hypothetical) depletant and the colloid + depletant system. The depletants were simplified as penetrable hard spheres. See the sketch in Fig. 3.12.

This theory has the advantage that the depletant concentrations in the coexisting phases follow directly from the (semi)grand potential which describes the colloid plus depletant system. As illustrated in Fig. 3.13, the system can arrange itself such as to provide a larger free volume for the depletants by overlap of two depletion

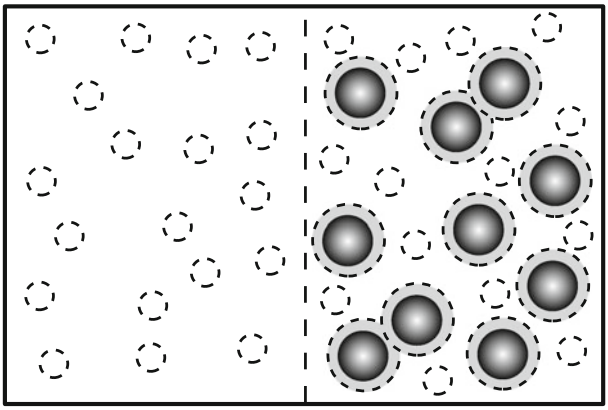

Fig. 3.12 A system (*right*) that contains colloids and penetrable hard spheres (*phs*) in osmotic equilibrium with a reservoir (*left*) only consisting of phs. A hypothetical membrane that allows permeation of solvent and phs but not of colloids is indicated by the *dashed line*. Solvent is considered as 'background'

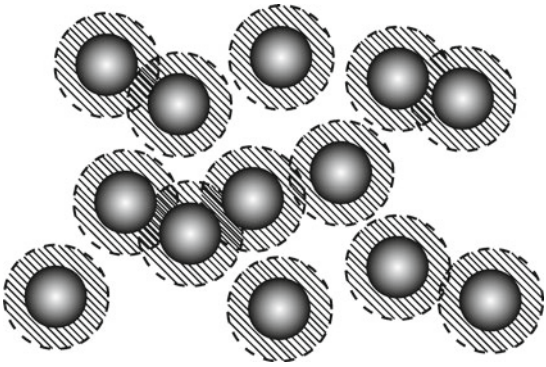

Fig. 3.13 Illustration of the free volume V_{free}: it is the unshaded volume not occupied by the colloids plus (partially overlapping) depletion layers

zones. This (entropic) physical origin of the phase transitions induced by depletion interactions is incorporated into the theory via the available volume for the depletants.

In FVT multiple overlap of depletion zones with thickness δ, see Fig. 3.14, is taken into account. Multiple overlap occurs for

$$\frac{\delta}{R} > \frac{2}{3}\sqrt{3} - 1 \simeq 0.15,$$

where three depletion zones start to overlap, see Fig. 3.14. Only for $\delta/R < 0.15$ is a colloid/depletant mixture pair-wise additive. For large δ/R a mixture of hard spheres plus penetrable hard spheres differs fundamentally from a mixture of hard-core spheres that directly attract one another [67]. This has a considerable influence on the

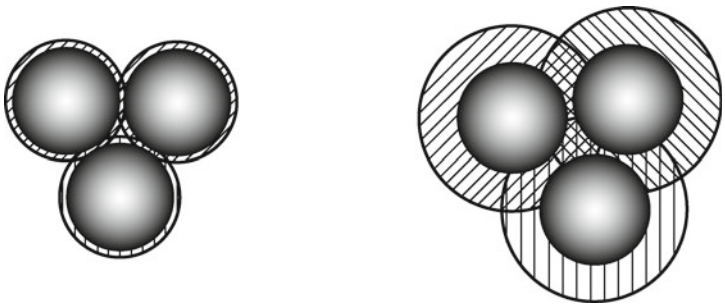

Fig. 3.14 Three hard spheres surrounded by depletion layers (*hatched areas*). When the depletion layers are thin (*left*) there is no multiple overlap of depletion layers; the system is pair-wise additive. For thicker depletion layers (*right*) multiple overlap of depletion layers occurs and depends on more than two-body contributions. The lowest value for δ/R where multiple overlap occurs follows from considering the triangle formed by the 3 particle centres; its edge is $2R + h$ at particle separation h. Multiple overlap starts when the *centre* of the triangle is a distance $R + \delta$ from the corners

topology of the phase diagram [68]. Multiple overlap of depletion layers widens the liquid window, which is the parameter range with phase transitions that include a stable liquid, in comparison with a pair-wise additive system [66].

The starting point of FVT is the calculation of the semigrand potential Ω describing the system of N_c colloidal spheres plus N_d depletants as depicted in Fig. 3.12.

$$\Omega(N_c, V, T, \mu_d) = F(N_c, N_d, V, T) - \mu_d N_d. \tag{3.53}$$

Using the thermodynamic relation

$$\left(\frac{\partial \Omega}{\partial \mu_d}\right)_{N_c,V,T} = -N_d, \tag{3.54}$$

one can write

$$\Omega(N_c, V, T, \mu_d) = F^0(N_c, V, T) - \int_{-\infty}^{\mu_d} N_d(\mu_d')\mathrm{d}\mu_d'. \tag{3.55}$$

Here $F^0(N_c, V, T)$ is the (Helmholtz) free energy of the colloidal hard sphere suspension without added depletant as given by Eq. (3.34) (fluid) or Eq. (3.38) (solid). Note that Eq. (3.55) is still exact and can be used (with approximations) to compute the phase behaviour of hard spheres plus interacting depletants (small hard spheres, interacting polymers, hard rods) [38, 66, 69]. Below only the case of non-interacting depletants is treated.

The essential step within FVT is the calculation of the number of depletants in the system of hard spheres + depletants as a function of the chemical potential μ_d imposed by the depletants in the reservoir. In the calculations presented below the colloidal hard spheres have a radius R and the depletants are described as penetrable hard spheres with radius δ.

For the calculation of N_d the Widom insertion theorem [70] is used according to which the chemical potential of the depletants in the mixture of hard spheres and depletants can be written as

$$\mu_d^S = \text{const} + k_B T \ln \frac{N_d}{\langle V_{\text{free}} \rangle}. \tag{3.56}$$

Here $\langle V_{\text{free}} \rangle$ is the ensemble-averaged free volume for the depletants in the system 'S' of hard spheres, illustrated in Fig. 3.13. The chemical potential of the depletants in the reservoir is simply

$$\mu_d^R = \text{const} + k_B T \ln n_d^R, \tag{3.57}$$

where n_d^R is the number density of the depletants in the reservoir 'R'. By equating the depletant chemical potentials Eqs. (3.56) and (3.57) the result

$$N_d = n_d^R \langle V_{\text{free}} \rangle \tag{3.58}$$

is obtained. The average free volume obviously depends on the volume fraction of the hard spheres in the system but also on the chemical potential of the depletants. The activity of the depletants affects the average configuration of the hard spheres. Now the key approximation is made to replace $\langle V_{\text{free}} \rangle$ by the free volume in the pure hard sphere dispersion $\langle V_{\text{free}} \rangle_0$:

$$N_d = n_d^R \langle V_{\text{free}} \rangle_0. \tag{3.59}$$

This expression is correct in the limit of low depletant activity but is only an approximation for higher depletant concentrations. Substituting the approximate Eq. (3.59) into Eq. (3.55) and using the Gibbs-Duhem relation,

$$n_d^R \mathrm{d}\mu_d = \mathrm{d}\Pi^R, \tag{3.60}$$

gives

$$\Omega(N_c, V, T, \mu_d) = F^0(N_c, V, T) - \Pi^R \langle V_{\text{free}} \rangle_0, \tag{3.61}$$

where $\Pi^R = n_d k_B T$ is the (osmotic) pressure of the depletants in the reservoir.

As expressions are available for the free energy of the hard sphere system (both in the fluid and solid state, see Sect. 3.3.2) and for the pressure of the reservoir, the only remaining quantity to calculate is $\langle V_{\text{free}} \rangle_0$. According to the Widom insertion theorem expressed in Eq. (3.56):

$$\mu_d = \text{const} + k_B T \ln \frac{N_d}{\langle V_{\text{free}} \rangle_0}. \tag{3.62}$$

The chemical potential μ_d can however also be written in terms of the reversible work W required for inserting a depletant into the hard sphere dispersion:

$$\mu_d = \text{const} + k_B T \ln \frac{N_d}{V} + W. \tag{3.63}$$

The free volume fraction α now follows from combining Eqs. (3.62) and (3.63):

$$\alpha = \frac{\langle V_{\text{free}} \rangle_0}{V} = e^{-W/k_B T}. \tag{3.64}$$

3.4.2 Scaled Particle Theory

An expression for the work of insertion W can be obtained from scaled particle theory (SPT) [71]. The work W is calculated is by expanding (scaling) the size of

the sphere to be inserted from zero to its final size: the radius of the scaled particle is $\lambda\delta$, with λ running from 0 to 1. In the limit $\lambda \to 0$, the inserted sphere approaches a point particle. In this limiting case it is very unlikely that the depletion layers overlap. The free volume fraction in this limit can therefore be written as

$$\alpha = 1 - \eta\left(1 + \frac{\lambda\delta}{R}\right)^3, \tag{3.65}$$

It then follows from Eq. (3.64) that

$$W = -k_B T \ln\left[1 - \eta\left(1 + \lambda\frac{\delta}{R}\right)^3\right] \quad \text{for } \lambda \ll 1. \tag{3.66}$$

In the opposite limit of a large inserted scaled particle $\lambda \gg 1$ the work of insertion W can be approximated as the volume work needed to create a cavity $\frac{4\pi}{3}(\lambda\delta)^3$ and is given by

$$W = \frac{4\pi}{3}(\lambda\delta)^3 \Pi^0 \quad \text{for } \lambda \gg 1, \tag{3.67}$$

where Π^0 is the (osmotic) pressure of the hard sphere dispersion. In SPT the above two limiting cases are connected by expanding W as a series in λ:

$$W(\lambda) = W(0) + \left(\frac{\partial W}{\partial \lambda}\right)_{\lambda=0}\lambda + \frac{1}{2}\left(\frac{\partial^2 W}{\partial \lambda^2}\right)_{\lambda=0}\lambda^2 + \frac{4\pi}{3}(\lambda\delta)^3 \Pi^0. \tag{3.68}$$

This yields

$$\begin{aligned}\frac{W(\lambda=1)}{k_B T} = &-\ln[1-\eta] + \frac{3q\eta}{1-\eta} \\ &+ \frac{1}{2}\left[\frac{6q^2\eta}{1-\eta} + \frac{9q^2\eta^2}{(1-\eta)^2}\right] \\ &+ \frac{\frac{4\pi}{3}q^3 R^3 \Pi^0}{k_B T}\end{aligned}, \tag{3.69}$$

where q is the size ratio between the depletant with radius δ and the hard sphere with radius R

$$q = \frac{\delta}{R}. \tag{3.70}$$

In Appendix, the result for the SPT osmotic pressure is derived:

$$\frac{\Pi^0 v_c}{k_B T} = \frac{\eta + \eta^2 + \eta^3}{(1-\eta)^3}. \tag{3.71}$$

Inserting Eq. (3.71) into Eq. (3.69) and using Eq. (3.64) yields

$$\alpha = (1-\eta)\exp[-Q(\eta)], \tag{3.72}$$

where

$$Q(\eta) = ay + by^2 + cy^3, \tag{3.73}$$

with $a = 3q + 3q^2 + q^3$, $b = \frac{9}{2}q^2 + 3q^3$ and $c = 3q^3$ and $y = \eta/(1-\eta)$. In Fig. 3.15 the free volume fraction α predicted by SPT (Eq. 3.72) is compared to computer simulation results on hard spheres plus penetrable hard spheres for $q = 0.1$ as a function of η. As can be seen the agreement is very good, as for other q values [72]. Now all ingredients are available to compile the semigrand potential Ω given by Eq. (3.61).

From Ω the total pressure of the hard spheres + phs and the chemical potential of the hard spheres in the hard sphere + depletant system at given μ_d^0 are obtained:

$$\Pi_{tot} = -\left(\frac{\partial \Omega}{\partial V}\right)_{N_c,T,\mu_d} = \Pi^0 + \Pi^R\left(\alpha - n_c\frac{\partial \alpha}{\partial n_c}\right) \tag{3.74}$$

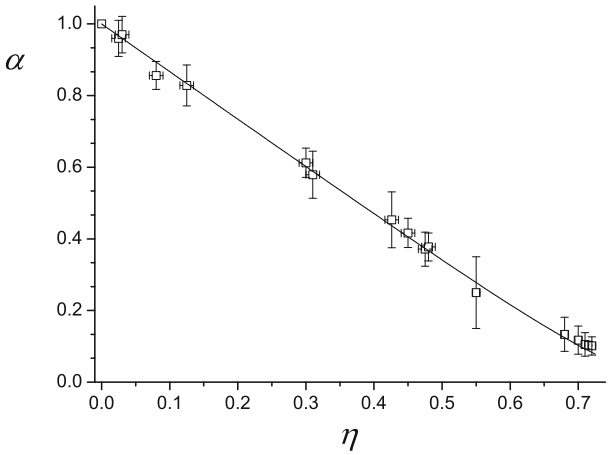

Fig. 3.15 Free volume fraction for penetrable hard spheres in a hard sphere dispersion for $q = \delta/R = 0.1$ as function of the hard sphere concentration. Data points are redrawn from Fortini et al. [50]. *Curve* is the SPT prediction of Eq. (3.72)

$$\mu_c = \left(\frac{\partial \Omega}{\partial N_c}\right)_{V,T,\mu_d} = \mu_c^+ - \Pi^R \frac{\partial \alpha}{\partial n_c}. \tag{3.75}$$

For non-interacting depletants Π^R is simply given by Van 't Hoff's law $\Pi^R = n_d^R k_B T$ or

$$\widetilde{\Pi}^R = \frac{\Pi^R v_c}{k_B T} = n_d^R v_d q^{-3} = \phi_d^R q^{-3} \quad , \tag{3.76}$$

with ϕ_d^R the relative reservoir depletant concentration $n_d^R v_d$, where v_d is the volume of a depletant sphere. These penetrable hard spheres can, by definition, freely interpenetrate each other. It is useful to define the overlap condition of phs by $n^* v_d = 1$. At $n^* = 1/v_d$ the spheres fill the available space but (on average) do not yet interpenetrate; this happens only for $n > n^*$. Hence one may write $\widetilde{\Pi} = \phi_d q^{-3}$, where ϕ_d is the concentration of penetrable hard spheres relative to overlap.

3.4.3 Phase Diagrams

The phase behaviour of a system of hard spheres and depletants can now be calculated by solving the coexistence equations for a phase I in equilibrium with a phase II

$$\mu_c^I(n_c^I, \mu_d) = \mu_c^{II}(n_c^{II}, \mu_d), \tag{3.77}$$

$$\Pi^I(n_c^I, \mu_d) = \Pi^{II}(n_c^{II}, \mu_d). \tag{3.78}$$

For numerical computations of phase coexistence, it is convenient to work with dimensionless quantities. The dimensionless version of the free volume expression Eq. (3.61) for the (semi) grand potential is

$$\widetilde{\Omega} = \widetilde{F}^0 - \alpha \widetilde{\Pi}^R, \tag{3.79}$$

where $\widetilde{\Omega} = \Omega v_c / k_B T V$.

The sketch of Fig. 3.8 can also be drawn for the semigrand potential ($\widetilde{\Omega}$ instead of $\widetilde{F}$) as a function of the colloid volume fraction for given depletant reservoir concentration and size ratio q. A first criterion for two coexisting binodal compositions is equality of the slope because it corresponds to the chemical potential. The chemical potential of the colloids $\widetilde{\mu}_c$ can generally be expressed using the standard thermodynamic relation

$$\widetilde{\mu}_c = \left(\frac{\partial \widetilde{\Omega}}{\partial \eta}\right)_{\widetilde{\Pi}^R,T,V}. \tag{3.80}$$

The (total) pressure is found from

$$\widetilde{\Pi}_{tot} = \eta \widetilde{\mu}_c - \widetilde{\Omega}. \tag{3.81}$$

When two compositions can be connected through the common tangent (the thin straight lines in Fig. 3.8 connecting these compositions), binodal points are found; the intercepts of the extrapolated lines correspond to the total pressure $\widetilde{\Pi}_{tot}$, see examples of scenarios for gas–liquid and fluid–solid coexistences in Fig. 3.8. For each depletant concentration the binodal compositions can be found in this manner; full phase diagrams can be constructed from such binodals.

For non-interacting depletants such as penetrable hard spheres the $\mu's$ and $\Pi's$ in the phase coexistence Eqs. (3.77) and (3.78) can be written such that binodal colloid concentrations follow from solving one equation with a single unknown [66] as for the hard-core Yukawa spheres discussed earlier. Equations (3.74) and (3.75) can be rewritten as

$$\tilde{\mu} = \tilde{\mu}^0 + \widetilde{\Pi}^R g(\eta) \tag{3.82}$$

$$\widetilde{\Pi}_{tot} = \widetilde{\Pi}^0 + \widetilde{\Pi}^R h(\eta), \tag{3.83}$$

where $g = -\partial\alpha/\partial\eta$ and $h = \alpha + g\eta$, giving the following explicit expressions for g and h:

$$g(\eta) = e^{-Q(\eta)}\left\{1 + [1+y][a + 2by + 3cy^2]\right\}, \tag{3.84}$$

$$h(\eta) = e^{-Q(\eta)}\left\{1 + ay + 2by^2 + 3cy^3\right\}. \tag{3.85}$$

The gas–liquid binodal can be solved from the second and third parts of

$$\widetilde{\Pi}^R = \frac{\tilde{\mu}_f^0(\eta_l) - \tilde{\mu}_f^0(\eta_g)}{g(\eta_g) - g(\eta_l)} = \frac{\widetilde{\Pi}_f^0(\eta_l) - \widetilde{\Pi}_f^0(\eta_g)}{h(\eta_g) - h(\eta_l)}, \tag{3.86}$$

where $\tilde{\mu}_f^0$ and $\widetilde{\Pi}_f^0$ are only a function of η, see Eqs. (3.30) and (3.33). Hence, Eq. (3.86) gives a unique relation $\eta_l(\eta_g)$ at given q. For some value of η_g, within the region of η_g values where a colloidal gas coexists with a colloidal liquid, the corresponding value of η_l follows from the second equality of Eq. (3.86). The corresponding binodal depletant reservoir pressure $\widetilde{\Pi}^R$ then follows from the first equality.

Similarly, the fluid-solid binodal can be obtained from

$$\widetilde{\Pi}^R = \frac{\tilde{\mu}_s^0(\eta_s) - \tilde{\mu}_f^0(\eta_f)}{g(\eta_f) - g(\eta_s)} = \frac{\widetilde{\Pi}_s^0(\eta_s) - \widetilde{\Pi}_f^0(\eta_f)}{h(\eta_f) - h(\eta_s)}, \tag{3.87}$$

where again $\tilde{\mu}_f^0$ is given by Eq. (3.33) and $\widetilde{\Pi}_f^0$ by Eq. (3.30); these are the fluid contributions. For colloidal dispersions in the solid state (fcc crystal) $\widetilde{\Pi}_s^0(\eta)$ and $\tilde{\mu}_s^0(\eta)$ are given by Eqs. (3.36) and (3.37), respectively.

Triple points have equal pressures and chemical potentials at colloidal gas, liquid *and* solid compositions. At the triple point expressions Eqs. (3.86) and (3.87) are connected through equal values for $\widetilde{\Pi}^R$ and, in principle, form a set of four equations from which the four coordinates of the triple point $(\eta_g, \eta_l, \eta_s, \widetilde{\Pi}^R)$ follow.

For large q ($q \geq 0.6$) the triple point can be approximated easily from Eqs. (3.82) and (3.83). The fluid-solid coexistence of the triple point occurs at nearly similar colloid concentrations as the pure hard sphere phase transition. For large q values, Eqs. (3.82) and (3.83) can be written as $\widetilde{\mu}_f = \widetilde{\mu}_f^0 = \widetilde{\mu}_s^0$ and $\widetilde{\Pi}_f = \widetilde{\Pi}_f^0 = \widetilde{\Pi}_s^0$, because $g(\eta)$ and $h(\eta)$ vanish for large q. In the coexisting colloidal gas phase the colloid concentration is then extremely small so $\widetilde{\Pi}_g = \widetilde{\Pi}^R$, since $h(\eta) \to 1$,

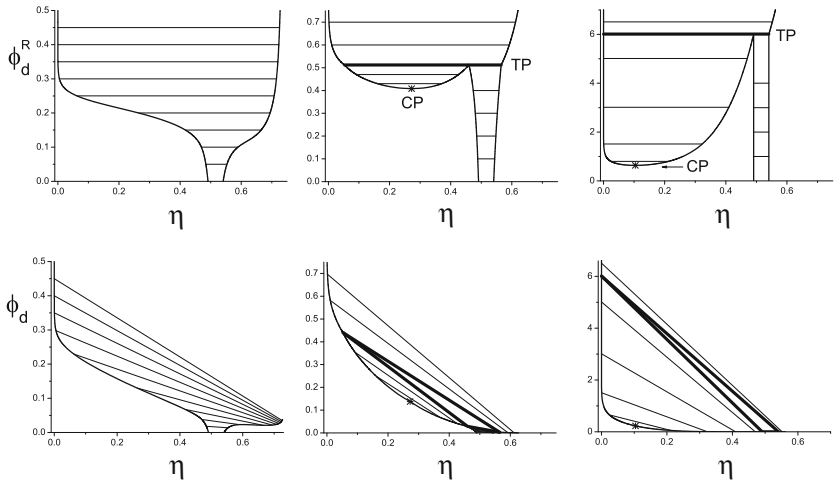

Fig. 3.16 Free volume theory predictions for the phase diagrams for hard spheres as depletants following Lekkerkerker et al. 1992 [35]. The *left* diagrams are for $q = 0.1$, *middle* $q = 0.4$, and *right* diagrams $q = 1.0$. *Upper* diagrams have depletant reservoir concentrations ϕ_d^R as ordinates, *lower* diagrams are in system depletant concentrations. *Triple lines* and *triangles* are indicated as *thick lines*. TP = triple point; CP = critical point (*asterisks* refer to the critical points). A few representative *tie-lines* are plotted as *thin lines*

implying $\widetilde{\Pi}^R = \widetilde{\Pi}_f^0 = \widetilde{\Pi}_s^0 = 6.01$ at the triple point. Hence, for large q the fluid-solid coexistence of the triple point occurs at nearly the same colloid concentrations as for the pure hard-sphere phase transition. The relative depletant concentration at the triple point now follows as $\phi_d^R \simeq \widetilde{\Pi}^R q^3 = 6.01 q^3$. As can be seen in Figs. 3.16 ($q = 1.0$) and 17 ($q = 0.6$) this is rather accurate.

The critical point can be found also as one equation in one unknown, for details, see [66]. The same applies to the *critical endpoint* (CEP), which corresponds to the q value where CP and TP coincide; it is the lowest q where a stable liquid is possible. See the extended discussions on liquid windows as related to the CEP in [66, 68].

In Fig. 3.16 phase diagrams are presented for $q = 0.1$, $q = 0.4$ and $q = 1.0$. As was already found by Gast et al. [30], for $q = 0.1$ there is only a fluid-crystal transition. For $\phi_d = 0$ the demixing gap is $0.491 < \eta < 0.541$ (see Sect. 3.3.2); with increasing depletant concentration this gap widens. For $q = 0.4$ there are a critical point (CP) and a triple point (TP) in the phase diagram, analogous to those found in simple atomic systems. At high depletant concentrations in the reservoir (above TP) a very dilute fluid (colloidal gas), coexists with a highly concentrated colloidal solid. Between TP and CP a colloidal gas (dilute fluid) coexists with a colloidal liquid (more concentrated fluid). At high volume fractions below the triple line, a colloidal liquid coexists with a colloidal solid phase. In the absence of depletant only the fluid-solid phase transition of a pure hard sphere dispersion remains. Increasing the depletant activity now plays a role similar to lowering the temperature in atomic systems. For larger q (see $q = 1.0$) the qualitative picture remains the same while the liquid window expands.

In the top diagrams of Fig. 3.16 the ordinate axis is the depletant concentration in the reservoir. The depletant concentrations in the system of coexisting phases can be obtained by using the relation

$$\phi_d = \alpha \phi_d^R.$$

Coexisting phases of course have the same μ_d and hence the same n_d^R but since the volume fractions of hard spheres and, hence, the free volume fractions α are different, n_d in the two (or three) phases are not the same, so the tie-lines are no longer horizontal. This is illustrated in the bottom diagrams of Fig. 3.16; now the ordinate axis gives the relative 'internal' or system concentrations ϕ_d. A few selected tie-lines are drawn to give an impression of depletant partitioning over the phases. Interestingly, the horizontal triple *line* in the presentation of the phase diagram at constant chemical potential μ_d (field-density representation) is now converted into a three-phase *triangle* system representation. The triple line connects three coexisting colloid concentrations at one fugacity (reservoir concentration).

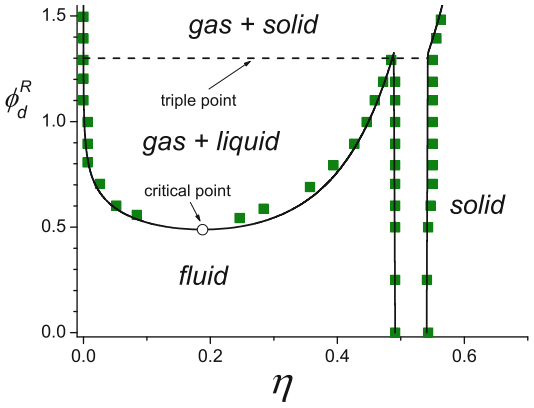

Fig. 3.17 Comparison of free volume theory (*curves*) with Monte Carlo computer simulations (data; [73]) for $q = 0.6$. *Open circle* = theoretical critical point

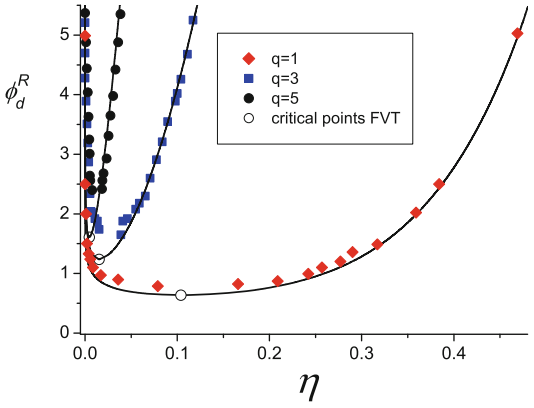

Fig. 3.18 Gas–liquid binodals for mixtures of HS + phs for large q values. *Curves* FVT; Data points: MC simulations by Dijkstra et al. [73] (q = 1) and Moncho-Jordá et al. [43] (q = 3 and q = 5)

In the system representation there are now three compositions (ϕ_d^1, η_g), (ϕ_d^2, η_l) and (ϕ_d^3, η_s). These three points in a (ϕ_d, η) plot form a triangle, within which there is three phase gas–liquid–solid coexistence.

As discussed in Sect. 3.3.2, the free volume theory is approximate in the sense that $\langle V_{free} \rangle$ is replaced by $\langle V_{free} \rangle_0$. To get an idea of the accuracy of the phase diagrams calculated with free volume theory the results for $q = 0.6$ are compared to computer simulations [73] in Fig. 3.17. The agreement is, given the fact that the free volume theory is approximate, very good. Also for q = 0.1 − 1.0 [73] and large q values [43] the agreement with simulations is striking. As a final illustration of the accuracy of FVT, colloidal gas–liquid binodals are plotted for q = 1, 3 and 5 in Fig. 3.18 and are compared to Monte Carlo computer simulation results.

Acknowledgments This text is highly inspired by several parts of the book I wrote with Henk Lekkerkerker and I thank him for the wonderful collaborations. I also acknowledge Agienus Vrij, Alvaro Gonzalez Garcia and Maartje S. Feenstra for useful discussions.

Appendix

As was the original objective of SPT [71], the pressure Π^0 of the hard sphere system can be obtained from the reversible work of inserting an identical sphere $(q = 1)$

$$\frac{W}{k_B T} = -\ln[1-\eta] + \frac{6\eta}{1-\eta} + \frac{9\eta^2}{2(1-\eta)^2} + \frac{4\pi R^3 \Pi^0}{3k_B T}, \tag{3.88}$$

to obtain the chemical potential of the hard spheres

$$\mu_c^0 = \text{const} + k_B T \ln \frac{N_c}{V} + W. \tag{3.89}$$

Applying the Gibbs-Duhem relation

$$\frac{\partial \Pi^0}{\partial n_c} = n_c \frac{\partial \mu_c^0}{\partial n_c}$$

one obtains

$$\frac{\Pi^0 v_c}{k_B T} = \frac{\eta + \eta^2 + \eta^3}{(1-\eta)^3}, \tag{3.90}$$

the SPT expression for the pressure of a hard sphere fluid [71], which preceded the slightly more accurate Carnahan-Starling equation Eq. (3.30), which contains an additional η^4-term.

References

1. F. Oosawa. *Hyo-Hyo Rakugaku*. Autobiography, Nagoya, 2005
2. S. Asakura, F. Oosawa, J. Chem. Phys. **22**, 1255 (1954)
3. D.H. Napper, *Polymeric Stabilization of Colloidal Dispersions* (Academix Press, Oxford, 1983)
4. As explained by Oosawa during the "Nagoya Symposium on Depletion Forces: Celebrating the 60th anniversary of the Asakura-Oosawa theory" held on March 14 and Japan 15 in 2014 in Nagoya
5. A. Vrij, Pure Appl. Chem. **48**, 471 (1976)
6. S. Asakura, F. Oosawa, J. Pol. Sci. **33**, 183 (1958)
7. R. Li-In-On, B. Vincent, F.A. Waite, ACS Symp. Ser. **9**, 165 (1975)
8. E. Eisenriegler, J. Chem. Phys. **79**, 1052 (1983)
9. A. Hanke, E. Eisenriegler, S. Dietrich, Phys. Rev. E **59**, 6853 (1999)
10. G.J. Fleer, A.M. Skvortsov, R. Tuinier, Macromolecules **36**, 7857 (2003)
11. H. De Hek, A. Vrij, J. Colloid Interface Sci. **84**, 409 (1981)
12. R. Fåhraeus, Physiol. Rev. **9**, 241 (1929)

13. R. Fåhraeus, Acta. Med. Scand. **55**, 1 (1921)
14. J.E. Thysegen, Acta Med. Scand. Suppl. **134**, 1 (1942)
15. J. Traube, Gummi Zeitung **39**, 434 (1925)
16. H.C. Baker, Inst. Rubber Ind. **13**, 70 (1937)
17. C.F. Vester, Kolloid Z. **84**, 63 (1938)
18. E. Dickinson, Food Hydrocolloids **17**, 25 (2003)
19. C. Sieglaff, J. Polym. Sci. **41**, 319 (1959)
20. C. Cowell, R. Li-In-On, B. Vincent, F.A. Waite, J. Chem. Soc. Faraday Trans. **74**, 337 (1978)
21. B. Vincent, P.F. Luckham, F.A. Waite, J. Colloid Interface Sci. **73**, 508 (1980)
22. B. Vincent, J. Edwards, S. Emmett, A. Jones, Colloids Surf. **17**, 261 (1986)
23. B. Vincent, Colloids Surf. **24**, 269 (1987)
24. B. Vincent, J. Edwards, S. Emmett, R. Croot, Colloids Surf. **31**, 267 (1988)
25. S. Hachisu, A. Kose, Y. Kobayashi, J. Colloid Interface Sci. **55**, 499 (1976)
26. A. Kose, S. Hachisu, J. Colloid Interface Sci. **55**, 487 (1976)
27. P.R. Sperry, H.B. Hopfenberg, N.L. Thomas, J. Colloid Interface Sci. **82**, 62 (1981)
28. P.R. Sperry, J. Colloid Interface Sci. **87**, 375 (1982)
29. P.R. Sperry, J. Colloid Interface Sci. **99**, 97 (1984)
30. A.P. Gast, C.K. Hall, W.B. Russel, J. Colloid Interface Sci. **96**, 251 (1983)
31. J.A. Barker, D. Henderson, Rev. Mod. Phys. **48**, 587 (1976)
32. A.P. Gast, W.B. Russel, C.K. Hall, J. Colloid Interface Sci. **109**, 161 (1986)
33. H.N.W. Lekkerkerker, Colloids Surf. **51**, 419 (1990)
34. H. Reiss, J. Phys. Chem. **96**, 4736 (1992)
35. H.N.W. Lekkerkerker, W.C.K. Poon, P.N. Pusey, A. Stroobants, P.B. Warren, Europhys. Lett. **20**, 559 (1992)
36. S.M. Ilett, A. Orrock, W.C.K. Poon, P.N. Pusey, Phys. Rev. E **51**, 1344 (1995)
37. F. Leal-Calderon, J. Bibette, J. Biais. Europhys. Lett. **23**, 653 (1993)
38. H.N.W. Lekkerkerker, R. Tuinier, *Colloids and the Depletion Interaction* (Springer, Berlin, 2011)
39. Y. Mao, M.E. Cates, H.N.W. Lekkerkerker, Phys. A **222**, 10 (1995)
40. E.J. Meijer, D. Frenkel, J. Chem. Phys. **100**, 6873 (1994)
41. M. Dijkstra, J.M. Brader, R. Evans, J. Phys. Condens. Matter **11**, 10079 (1999)
42. P.G. Bolhuis, A.A. Louis, Macromolecules **35**, 1860 (2002)
43. A. Moncho-Jordá, A.A. Louis, P.G. Bolhuis, R. Roth, J. Phys. Condens. Matter **15**, S3429 (2003)
44. D. Kleshchanok, R. Tuinier, P.R. Lang, *J. Phys Condens. Matt.* **20**, 073101 (2008)
45. J.D. van der Waals, Doctoral thesis. A.W. Sijthoff, Leiden, 1873
46. D.A. McQuarrie, *Statistical Mechanics* (University Science Books, Sausalito, 2000)
47. A. Malijevský, J. Kolafa. *Introduction to the Thermodynamics of Hard Spheres and Related Systems, in: 'Theory and Simulation of Hard-Sphere Fluids and Related Systems',* Lecture Notes in Physics, vol 753 (Springer, Berlin, 2008)
48. N.F. Carnahan, K.E. Starling, J. Chem. Phys. **51**, 635 (1969)
49. J.-P. Hansen, I.R. McDonald, *Theory of Simple Liquids* (Academic Press, San Diego, 1986)
50. A. Fortini, M. Dijkstra, R. Tuinier, *J. Phys. Condens. Matt.* **17**, 7783–7803 (2005)
51. W.G. Hoover, F.H. Ree, J. Chem. Phys. **49**, 3609 (1968)
52. J.E. Lennard-Jones, A.F. Devonshire, Proc. Roy. Soc. **163A**, 53 (1937)
53. D. Frenkel, A.J.C. Ladd, J. Chem. Phys. **81**, 3188 (1984)
54. C.G. de Kruif, P.W. Rouw, J.W. Jansen, A. Vrij, J. de Phys. **46**, C3–295 (1985)
55. P.N. Pusey, W. Van Megen, Nature **320**, 340 (1986)
56. J. Levelt Sengers, *How Fluids Unmix* (Edita KNAW, Amsterdam, 2002)
57. Y. Tang, B.C.-Y. Lu, J. Chem. Phys. **99**, 9828 (1993)
58. Y. Tang, J. Chem. Phys. **118**, 4140 (2003)
59. Y. Tang, Y.-Z. Lin, Y.-G. Li, J. Chem. Phys. **122**, 184505 (2005)
60. R. Tuinier, G.J. Fleer, J. Phys. Chem. B **110**, 2045 (2006)
61. K.P. Shukla, J. Chem. Phys. **112**, 10358 (2000)

62. M. Dijkstra, Phys. Rev. E **66**, 021402 (2002)
63. J.M. Brader, R. Evans, M. Schmidt, Mol. Phys. **101**, 3349 (2003)
64. M. Fuchs, K.S. Schweizer, J. Phys. Condens. Matter **14**, R239 (2002)
65. P.G. Bolhuis, A.A. Louis, J.P. Hansen, Phys. Rev. Lett. **89**, 128302 (2002)
66. G.J. Fleer, R. Tuinier, Adv. Colloid Interface Sci. **143**, 1–47 (2008)
67. R. Tuinier, M.S Feenstra. *Langmuir* (2014). doi:10.1021/la5023856
68. G.J. Fleer, R. Tuinier, Phys. A **379**, 52 (2007)
69. D.G.A.L. Aarts, R. Tuinier, H.N.W. Lekkerkerker, J. Phys. Condens. Matter **14**, 7551 (2002)
70. B. Widom, J. Chem. Phys. **39**, 2808 (1963)
71. H. Reiss, H.L. Frisch, J.L. Lebowitz, J. Chem. Phys. **31**, 369 (1959)
72. E.J. Meijer, Computer Simulation of Molecular Solids and Colloidal Dispersions, PhD thesis. Utrecht University, Utrecht, 1993
73. M. Dijkstra, R. van Roij, R. Roth, A. Fortini, Phys. Rev. E **73**, 041409 (2006)